Multicharged Ion Impact on Clean Au(111): Suppression of Kinetic Electron Emission in Glancing Angle Scattering

C. Lemell,[1] J. Stöckl,[1] J. Burgdörfer,[2] G. Betz,[1] HP. Winter,[1] and F. Aumayr[1,*]

[1]*Institut für Allgemeine Physik, TU Wien, Wiedner Hauptstrasse 8-10, A-1040 Vienna, Austria*

[2]*Institut für Theoretische Physik, TU Wien, Wiedner Hauptstrasse 8-10, A-1040 Vienna, Austria*

(Received 16 April 1998)

We have measured the number statistics of emitted electrons in coincidence with the projectile scattering angle distribution for multiply charged slow Ar ions scattered off an Au(111) surface at grazing incidence. The comparison of the electron statistic spectra for different projectile exit and incidence angles permits a separation of potential and kinetic electron emission. A molecular dynamics simulation allows to associate the multiple electron emission with specific trajectory histories (planar and subsurface channeling, close collisions with target atoms at steps and imperfections). [S0031-9007(98)06964-6]

PACS numbers: 79.20.Rf, 61.85.+p, 79.60.Bm

The interaction of slow highly charged ions (HCI) with clean surfaces reveals new phenomena like the transient formation of exotic "hollow atoms" [1–5] and the recently discovered effect of "potential sputtering" [6]. Above the surface the formation and evolution of hollow atoms can be described theoretically by the classical over-the-barrier (COB) model [1,7]. The image energy gain and the distance of hollow atom formation predicted by this model could be verified in several independent experiments [8–10]. Other signatures of hollow atom formation and decay like potential electron emission (PE) [11] are often masked by significant contributions from below surface interaction processes, in particular, at higher projectile energies where kinetic emission phenomena become dominant [12]. So far, most such results could therefore be used only as indirect proof for the COB model. We have developed an experimental approach which enables us to distinguish between electron emission induced above (or at) the surface from below surface emission. This information can, in turn, provide distinction between kinetic and potential emission.

In this work we correlate the electrons emitted during grazing incidence scattering of multiply charged argon ions at a clean metal surface with specific projectile trajectories characterized by the resulting scattering angle, to achieve a separation of above and below surface emission. A comparison with electron emission data for normal incidence with the same projectile, charge state, and target species having equal velocity normal to the surface allows the direct identification of potential and kinetic electron emission near the KE threshold.

The measurements have been carried out using multiply charged Ar^{q+} ($q \leq 9$) ions produced in a 5 GHz electron cyclotron resonance ion source [13] at TU Wien. The ion source provides projectiles with energies up to $10 \times q$ keV where q is the charge state of the extracted ions. These ions are focused to a beam, mass analyzed, and transported to a differentially pumped UHV chamber (10^{-10} mbar). The experimental setup is shown schematically in Fig. 1. The incident ion beam is collimated to 1 mm in diameter and directed onto a Au(111) single crystal target which is mounted on a manipulator that allows one to adjust the ion impact angle ψ. The target is prepared by cycles of sputtering under various angles with 1–5 keV Ar^+ ions and successive annealing at about 500 °C [9].

The angular distribution of projectiles scattered off the target surface under a grazing angle of incidence (typically 5°) as well as a small part of the primary beam are recorded on a position-sensitive channel plate detector (PSD) equipped with a two-dimensional wedge and strip anode. Electrons emitted from the ion-surface interaction region are extracted by a weak electric field through a highly transparent grid and accelerated onto a surface barrier type detector biased at +25 kV. The number of electrons emitted in a particular ion impact event [the electron number statistics (ES) giving access to the total electron yield γ] is deduced from the detectors pulse height distribution in the usual way [11,14]. According to ray-trace calculations performed for our geometry with the program MacSIMION and subsequent experimental checks, a field

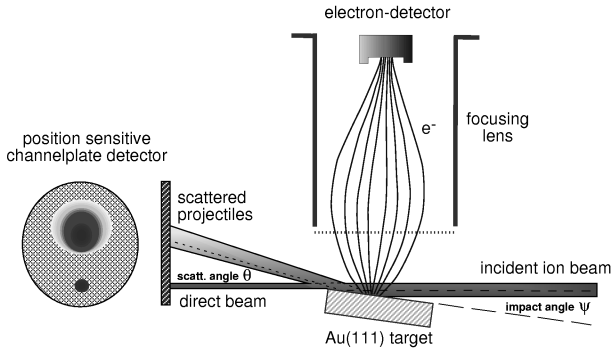

FIG. 1. Experimental setup (schematically) for measuring electron emission from grazing incidence HCI-surface interaction in coincidence with scattered projectiles (cf. text).

of about 100 V/cm is sufficient to collect all electrons with energies below 50 eV emitted into the solid half angle. The influence of this extraction field (resulting in a slightly larger impact angle and a displacement of the direct beam on the PSD) has been taken into account by correcting the angle of incidence and the position of the direct beam. The position signals from the ion detector and the pulse height signal from the electron detector are amplified, delayed in time, and fed into a multiparameter analog-to-digital converter system. This system is triggered by a fast gate signal produced from events on either ion or electron detector and therefore allows the storage of both coincident and noncoincident events. A first description of our setup has been given in Ref. [15]; more technical details will be presented elsewhere [16]. Other coincidence techniques have been successfully applied to ion-surface interaction studies (see, e.g., [17]).

In Fig. 2a the intensity distribution of scattered projectiles, as recorded on the PSD, is shown for 0.45 keV/amu Ar^{8+} ions impinging under a grazing angle of $\psi = 5°$ onto a Au(111) single crystal surface (random azimuthal orientation). For this choice of parameters, the velocity parallel to the surface of $v_{\parallel} \approx 0.13$ a.u. is slightly above the threshold for kinetic emission in binary encounter collisions with conduction electrons [18]. The normal component of the energy, $E_{\perp}$, however, is very low ($E_{\perp} =$ 137 eV or 3.4 eV/amu) corresponding to a velocity along the surface normal of $v_{\perp} = 1.2 \times 10^{-2}$ a.u. The perpendicular velocity is thus within a factor of 3 of the lower bound given by the image acceleration of the projectile. For such a low velocity, electron emission is exclusively caused by the potential energy of the projectiles.

The needlelike feature on the right-hand side of Fig. 2a represents the small fraction of the primary ion beam that has passed above the target (cf. Fig. 1), while the broader peak represents the scattered projectiles. The width of the scattering distribution ($\pm 2.5°$), in particular, the asymmetry towards larger scattering angles, points to imperfections in the Au(111) surface [19]. Projectiles scattered from the collective planar potential ("surface channeling" [9]) of an ideally flat surface are specularly reflected and would contribute only to the central peak (dark region) of the angular distribution while those scattered from surface imperfections (e.g., steps) or projectiles undergoing subsurface channeling can be found in the wings of the scattering distribution. The asymmetry in Fig. 2b is due to the fact that a small part of the scattering distribution is outside of the active area of our PSD. The resulting data presented in Figs. 3a–3c are, however, not influenced by this technical detail.

One multiply charged ion can eject up to 40 electrons (with a mean number of about 19 electrons per ion), as can be seen from the total ES spectrum shown in Fig. 3a. This noncoincidently measured spectrum features an unusually broad ES distribution that is indicative of a superposition of different scattering processes. Note that a specific feature of the multiplicity spectra such as

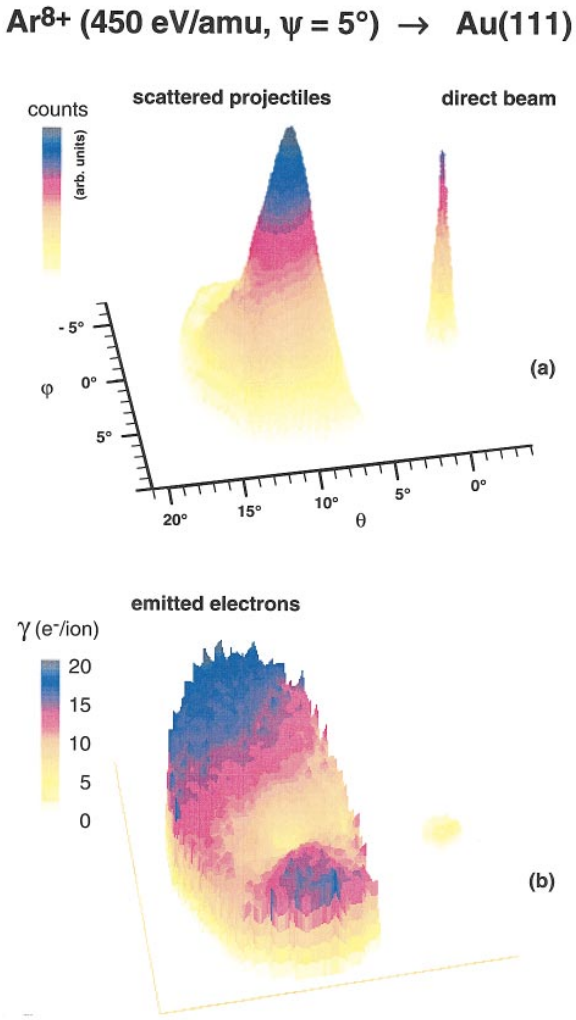

FIG. 2(color). (a) Intensity distribution of scattered projectiles as recorded on the position sensitive detector for the case of 0.45 keV/amu Ar^{8+} ions impinging under a grazing angle of 5° onto a Au(111) single crystal surface (cf. text). (b) Mean number of emitted electrons associated with projectile scattering under various exit angles [positions correspond to (a)].

shown in Fig. 3 is that they are capable of providing direct information on both *alternative* and *additive* reaction channels (in the present case, *alternative* channels include bulk penetration without reflection, large angle scattering, and a field emission background at low electron numbers [14], while an example for *additive* channels are PE and KE). The ES spectrum changes drastically when scattered projectiles are detected in coincidence near the direction of specular reflection. Apart from the suppression of field emission, the mean number of emitted electrons has shifted to 17 electrons/ion and a decrease in the number of high electron multiplicity events is clearly evident. Those high multiplicity events are therefore associated with projectiles deeply penetrating the target or leaving it under scattering angles too large to be detected by our setup.

The correlation between the multiplicity spectrum and the projectile scattering angle can be investigated in further

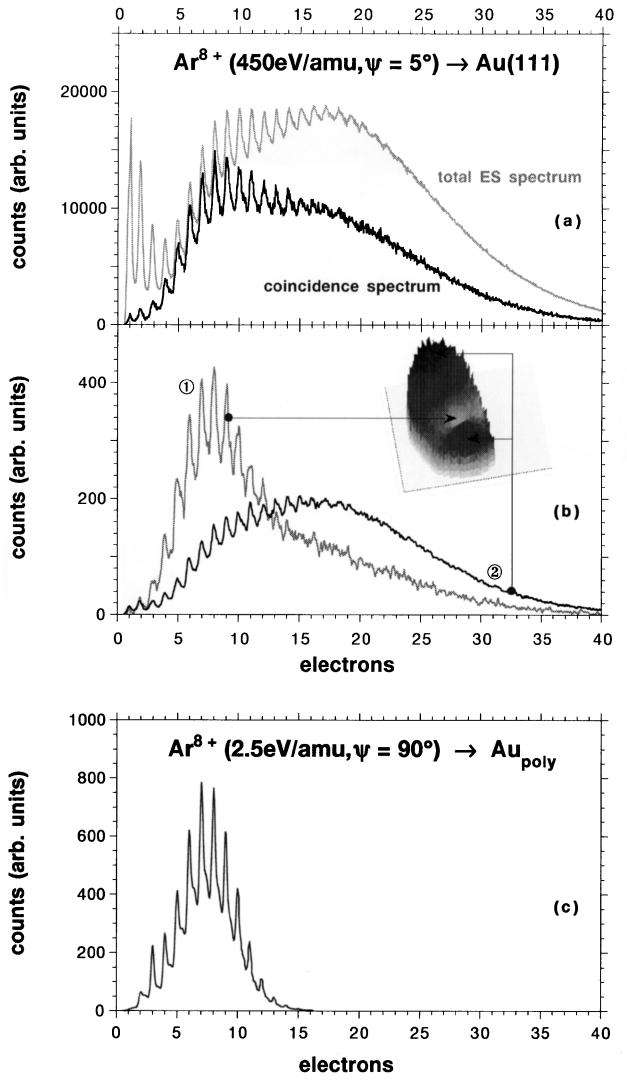

FIG. 3. (a) Total (noncoincidence) and coincidence ES (electron emission statistic) spectra for the case of 0.45 keV/amu Ar^{8+} ions impinging under a grazing angle of 5° onto a Au(111) single crystal surface. (b) ES spectra in coincidence with the central part (1) and with the wings of the scattering distribution (2); see inset. (c) For comparison: ES spectrum obtained for 2.5 eV/amu normal incidence Ar^{8+} projectiles on polycrystalline Au (from Ref. [11]).

detail by selecting coincidences with different portions of the scattered particle distribution. Figure 2b (also the inset of Fig. 3b) shows the mean number of electrons (i.e., the total electron yield γ) as a function of the two-dimensional angular distribution of the scattered projectiles. A pronounced minimum with $\gamma < 10$ appears precisely where the scattered particle distribution peaks, i.e., at the specular reflection angle. Particles emerging at larger scattering angles (wings of the scattering distribution) cause emission of a considerably larger number of electrons.

The ES spectra in coincidence with the central (labeled in the following as 1) and peripheral (labeled 2) parts of the reflected particle distribution (see Fig. 3b) represent different processes whose superposition gives rise to the broad ES spectrum shown in Fig. 3a. To identify the origin of the different ES spectra we compare this ES spectrum with the spectrum for normal incidence (Fig. 3c) and the same total velocity as the normal component of the specular reflected particle. The remarkable observation is now that normal incident ES spectrum and grazing incident ES spectrum of surface channeled projectiles give practically identical ES spectra near the maximum (below we comment on the tail towards higher multiplicities, seen in ES spectrum 1 of Fig. 3b). This component can therefore be unambiguously correlated to potential emission. Note that any *additional* kinetic emission of n electrons on top of the potential emission would shift the maximum of the ES spectrum by n units to the right. For projectiles undergoing specular reflection, however, Figs. 3b and 3c indicate that $n \leq 1$; i.e., kinetic emission is strongly suppressed. Moreover, based on finite temperature molecular dynamics (MD) simulations we can attribute this part of the ES spectrum to "above" surface (including "at surface" [20]) emission from projectiles which did not penetrate the surface and thus did not approach the topmost layer closer than to a distance of about 1 a.u. (0.5 Å). The fact that the ES spectra in Figs. 3b and 3c are nearly identical near the maximum at $n = 8$ despite vastly different parallel velocities shows that the above-surface PE is independent of the parallel velocity $v_{\parallel}$.

The high-multiplicity spectrum 2 in Fig. 3b can, in turn, be attributed to the sum of potential and kinetic emission. Kinetic emission includes both binary encounter type collisions between the projectile and conduction electrons as well as quasimolecular promotion in close ion-atom or atom-atom collisions. The characteristic differences in the multiplicity for specularly reflected projectiles (undergoing only distant collisions) and projectiles scattered into larger angles (closer collisions) permit to further distinguish these processes. Note, however, that the impact parameters are still relatively large compared to inner shell radii. Promotion of inner shells which plays an important role for stopping power thresholds [21,22] is in the present case of minor importance. Rather, the multiple scattering at a large number of target atoms at intermediate impact parameters ($1 \leq b \leq 2$ a.u.) appears to be responsible for the ejection of about *10 additional electrons* on top of the potential electron emission.

We can describe the kinetic emission process by assuming a yield of electrons per collision as a function of the impact parameter b of the form

$$Y(b) = Y_0 e^{-b/b_c} \tag{1}$$

and sum over all contributions from the complete collision history along a given trajectory. The free parameters in Eq. (1) can be determined from the distribution of the pure kinetic emission (distribution 2 in Fig. 3b) after subtraction of γ_{PE} for potential emission.

In Fig. 4 we display the simulated ES spectrum for an ideal surface and for a surface with steps and defects calculated according to Eq. (1) along the trajectories of a MD

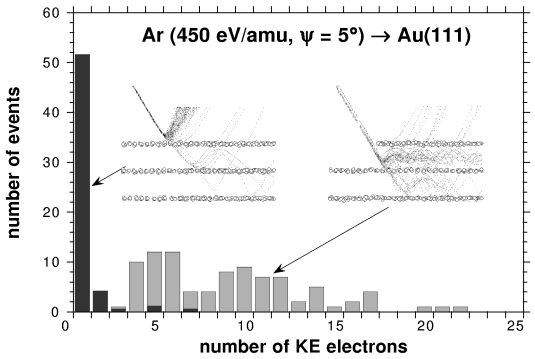

FIG. 4. Multiplicity distribution due to kinetic emission calculated according to Eq. (1) along the trajectories of a MD ensemble for an ideal surface (left) and a stepped surface (right).

ensemble. For a choice of $Y_0 = 0.5$ and $b_c \approx 1.3$ a.u. we find good qualitative agreement with the kinetic emission component of the ES spectrum (Fig. 3). For an ideal surface, kinetic emission is strongly suppressed ($n \leq 1$) while scattering with steps, etc., leads to the emission of a large number of electrons. The surprising aspect is that this is *not* due to closer collisions with smaller impact parameters but due to the drastically increased interaction length and collision number with very similar impact parameter distributions. The value for b_c is close to the radius of the $5d$ shell in Au ($\langle r \rangle_{5d} \approx 1.4$ a.u.). We therefore conclude that kinetic emission involves predominantly the $5d$ electrons of Au, i.e., the lower portion of the conduction band. It is worth noting that the emission process is not necessarily of the binary encounter type. Quasimolecular potential energy diagrams for the ion-atom collision system Ar-Au indicate promotion of the $5d$ level to near zero binding energy at comparable distances ($r_c \sim 1.2$ a.u.) [23].

Finally, the weak high multiplicity component in the ES spectrum (spectrum 1 in Fig. 3b) is most likely due to projectiles first giving rise to PE and then undergoing a sequence of multiple collisions (steps, defects, subsurface channeling), but ending up "accidentally" at the specular angle. These will provide contributions to the high multiplicity wing of the glancing angle distribution.

In summary, we have presented an unambiguous decomposition into potential and kinetic electron emission in multiply charged ion-surface scattering at grazing incidence. We have shown that potential electron emission is completely governed by the value of the perpendicular velocity component $v_\perp$ and is independent of the parallel velocity. Kinetic emission is strongly suppressed for "ideal" glancing angle trajectories. Collisions with surface steps (imperfections as well as subsurface channeling) provide the dominant contribution to the kinetic emission with multiplicities up to 25 electrons/ion.

This work has been supported by Austrian Fonds zur Förderung der Wissenschaftlichen Forschung (P 10164, P 12470) and by Österreichische Nationalbank (Jubiläumsfondsprojekt 5911).

*Corresponding author.
Email address: aumayr@iap.tuwien.ac.at

[1] J. Burgdörfer *et al.*, Phys. Rev. A **44**, 5647 (1991); J. Burgdörfer, in *Fundamental Processes and Applications of Atoms and Ions*, edited by C. D. Lin (World Scientific, Singapore, 1993), pp. 517–614.
[2] F. Aumayr and HP. Winter, Comments At. Mol. Phys. **29**, 275 (1994).
[3] A. Arnau *et al.*, Surf. Sci. Rep. **27**, 113 (1997), and references cited therein.
[4] J. Das and R. Morgenstern, Comments At. Mol. Phys. **29**, 205 (1993).
[5] N. Stolterfoht *et al.*, Phys. Rev. A **52**, 445 (1995).
[6] T. Neidhart *et al.*, Phys. Rev. Lett. **74**, 5280 (1995); M. Sporn *et al.*, Phys. Rev. Lett. **79**, 945 (1997).
[7] C. Lemell *et al.*, Phys. Rev. A **53**, 880 (1996).
[8] F. Aumayr *et al.*, Phys. Rev. Lett. **71**, 1943 (1993).
[9] H. Winter *et al.*, Phys. Rev. Lett. **71**, 1939 (1993).
[10] F. W. Meyer *et al.*, Nucl. Instrum. Methods Phys. Res., Sect. B **98**, 441 (1995).
[11] H. Kurz *et al.*, Phys. Rev. Lett. **69**, 1140 (1992); Phys. Rev. A **48**, 2182 (1993).
[12] M. Rösler and W. Brauer, in *Particle Induced Electron Emission*, edited by I. G. Höhler (Springer, Berlin, 1991), Vol. 122.
[13] M. Leitner *et al.*, Rev. Sci. Instrum. **65**, 1091 (1994).
[14] F. Aumayr *et al.*, Appl. Surf. Sci. **47**, 139 (1991).
[15] C. Lemell *et al.*, Nucl. Instrum. Methods Phys. Res., Sect. B **125**, 146 (1997).
[16] C. Lemell, Ph.D. thesis, TU Wien (unpublished); C. Lemell *et al.* (to be published).
[17] V. A. Morosov *et al.*, Nucl. Instrum. Methods Phys. Res., Sect. B **98**, 597 (1995); Rev. Sci. Instrum. **67**, 6 (1996).
[18] E. V. Alonso *et al.*, Phys. Rev. B **22**, 80 (1980); Surf. Sci. **166**, L155 (1986); G. Lakits *et al.*, Phys. Rev. A **42**, 5780 (1990).
[19] R. Pfandzelter, Phys. Rev. B **57**, 15 496 (1998).
[20] J. Burgdörfer *et al.*, Nucl. Instrum. Methods Phys. Res., Sect. B **98**, 415 (1995).
[21] J. W. Rabalais *et al.*, Phys. Rev. Lett. **69**, 1391 (1992).
[22] P. Kürpick, Phys. Rev. B **56**, 6446 (1997).
[23] P. Kürpick (private communication).